

SINGLE-INPUT PLANAR NAVIGATION VIA PROPORTIONAL HEADING CONTROL EXPLOITING NONHOLONOMIC MECHANICS OR VORTEX SHEDDING

Michael J. Fairchild

Department of Mathematics and Statistics
University of North Carolina at Charlotte
Charlotte, North Carolina 28223

Peter M. Hassing

Scott David Kelly*

Parthesh Pujari

Phanindra Tallapragada

Department of Mechanical Engineering and Engineering Science
University of North Carolina at Charlotte
Charlotte, North Carolina 28223

ABSTRACT

We present a strategy for coupled steering and motion generation applicable to a class of single-input planar robotic vehicles. We demonstrate this strategy through simulations of two different vehicles under closed-loop control, the first a novel variation of the Chaplygin sleigh and the second a fishlike swimmer in an ideal fluid. The dynamics of the former are influenced by a nonholonomic constraint and the dynamics of the latter by a hydrodynamic force associated with vortex shedding. The juxtaposition of these two systems highlights a link between nonholonomic mechanics and hydrodynamics explored in a prior paper.

1 INTRODUCTION

In this paper we describe an approach to planar motion control for a class of underactuated robotic systems governed by nonlinear dynamics. We present two examples of such systems, one a terrestrial vehicle subject to a nonholonomic constraint and the other an aquatic vehicle coupled to a surrounding fluid through localized vortex shedding. The parallel treatment of these two systems underscores a phenomenological link between nonholonomic mechanics and fluid-body interactions previously explored in [1].

Each of the vehicles we consider exhibits a solitary internal degree of freedom, assumed to be actuated directly. In each case, manipulation of this degree of freedom is sufficient to mediate the vehicle's heading in the plane. The dynamics of each vehicle

are such that oscillations in heading produce longitudinal translation.

The first vehicle is depicted in Fig. 1. A cart is supported by casters in the front and by a single wheel in the rear, the wheel aligned with the cart's longitudinal direction. The wheel is assumed to roll without slipping, so that lateral motion of the cart's rear is prohibited. A mass is affixed to the cart in a manner that permits lateral motion between the two. In Fig. 1, the mass is shown atop a planar pendulum that swings laterally to correspond with a physical system described in Section 4, but we consider the dynamics of the system only in the plane parallel to the ground, so the mechanism for moving the mass is immaterial.

The panel on the right of Fig. 1 depicts a frame from a simulation of the cart, viewed from above, subject to a simple form of feedback control. A desired value for the cart's heading, defined as the angle between the cart's longitudinal axis and the spatially fixed horizontal axis, is specified as a function of time. The discrepancy between the current heading and the desired heading is multiplied by a constant gain, and the lateral acceleration of the mass relative to the cart is set equal to their product.

In the simulation shown, the cart began at rest at the origin, aligned with the vertical axis to correspond with the desired heading $\theta_{\text{desired}}(0) = \pi/2$. A step change in the desired heading occurred thereafter, decreasing $\theta_{\text{desired}}(t)$ to 1.4. The resulting path of the cart's center of mass is overlaid with the cartoon. Initial lateral oscillations in the cart's position decay as the cart accelerates toward a constant translational speed.

The mechanics of the cart are such that the closed-loop sys-

*Address all correspondence to this author at scott@kellyfish.net.

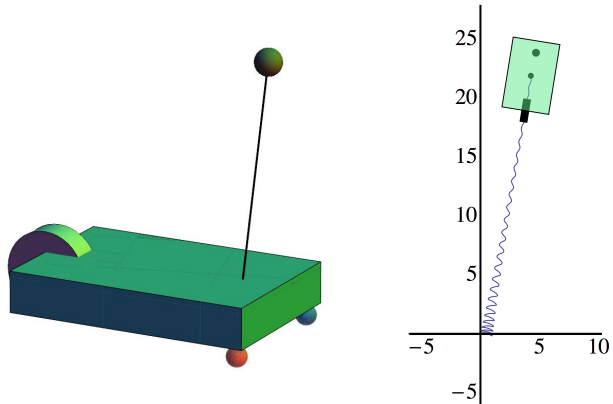


Figure 1. ACCELERATION FROM REST OF A CART USING THE LATERAL DISPLACEMENT OF A MASS TO REGULATE ITS HEADING.

tem, using proportional heading control with an arbitrarily selected controller gain, achieves the desired average heading in Fig. 1 with no steady-state error. A different choice of gain provides the same average heading control, but generates a response to the same step input that results in a different asymptotic rolling speed. This suggests a simple approach to planar motion-planning for this system, at least within a certain range of system parameters, initial conditions, and performance goals. If the goal is to move in a certain direction at a certain speed, the former can be achieved via proportional control applied to the lateral acceleration of the mass, while the latter can be achieved by manipulating the feedback gain.

Fig. 2 depicts the second vehicle we consider. A planar hydrofoil, representing a simple model for a fishlike swimmer, is surrounded by an infinite inviscid fluid with equal density, at rest infinitely far away. Variations in the foil’s camber allow the foil to propel itself by exploiting interactions between inertial effects manifest in the foil’s shape-dependent effective inertia and the effects of vortex shedding from the foil’s trailing point, the latter enabled by the periodic application of a *Kutta condition* [2] at this point.

The panel on the left of Fig. 2 depicts a frame from a simulation analogous to the simulation from Fig 1. At the start of the present simulation, the foil was situated at rest, aligned with the horizontal axis. A step change in the foil’s desired heading, calling for a left turn of .3 radians, elicited a response from a controller specifying the rate of change of the foil’s camber to be proportional to the heading error. At the instant shown, the foil’s heading exhibits decaying oscillations about the desired direction, while the foil’s translational speed approaches a value determined by the feedback gain. Dots shown in the foil’s wake represent individual point vortices; the dots are colored and scaled according to vortex orientation and strength. Note that vortices shed by the foil roll up dynamically into the inverse Kármán vortex street characteristic of real fishlike swimming [3].

The panel on the right of Fig. 2 illustrates the dependence of the foil’s asymptotic translational speed on the proportional

feedback gain k_p , depicting the speed of the foil’s center as a function of time for two different values of this gain. Since the oscillations in heading depicted in Fig. 2 decay more slowly than those depicted in Fig. 1, we note that even if oscillations in the foil’s shape persist indefinitely, the foil’s translational speed will approach a constant value, below which the foil’s oscillations produce net thrust and above which they produce net drag.

In what follows, we examine both of the systems described above in greater detail. The control paradigm that serves as the paper’s theme resulted from the authors’ search for a simple approach to steering a robotic version of the fishlike swimmer in Fig. 2. The physical system is shown in Fig. 6. In fact, while the method we propose exhibits limitations in its applicability to the robotic cart, simulations using the model depicted in Fig. 2 indicate unanimously that proportional heading control can be used to achieve even large changes in direction with zero steady-state error, and can be used effectively to mediate swimming speed without changes in direction.

At the beginning of this Introduction, we noted that mechanical systems subject to nonholonomic constraints exhibit basic dynamic similarities to systems in which bodies and fluids are coupled through vortex shedding. It is our view that the two classes of systems are related on a fundamental level, in that the role played by vortex shedding in real fluid-body interactions may be idealized in terms of integrable and nonintegrable constraints, but it’s not for this reason alone that we juxtapose the two systems in this paper.

Our perspective on robotic locomotion as a topic at the interface of geometric mechanics and nonlinear control has its roots in papers like [4] and [5], which developed a theory of driftless locomotion for systems capable of generating *geometric phase* by periodically varying multiple internal degrees of freedom. The subsequent development, in papers like [6] and [7], of a geometric analysis for systems capable of accumulating propulsive momentum by exploiting nonholonomic constraints — in other words, systems that were no longer driftless in the control-theoretic sense — was built upon examples in which geometric phases and dynamic phases both contributed to locomotion. In focusing on systems with single internal degrees of freedom, we isolate the problem of generating dynamic locomotion from the problem of generating geometric phase, the latter feasible only for multi-input systems.

2 CART WITH A MOVING MASS

Without the pendulum on top, the cart shown in Fig. 1 represents a variation of the *Chaplygin sleigh*, a canonical nonholonomic system studied by its namesake in [8]. The constraint on the system is typically taken to represent the resistance of a vertical blade to lateral sliding; we imagine a wheel in place of the blade — neglecting the contribution of the wheel’s rotation to the system’s total kinetic energy — to match our model with robotic realizations of the device like that pictured in Fig. 6.

The control of a Chaplygin sleigh with a movable mass on

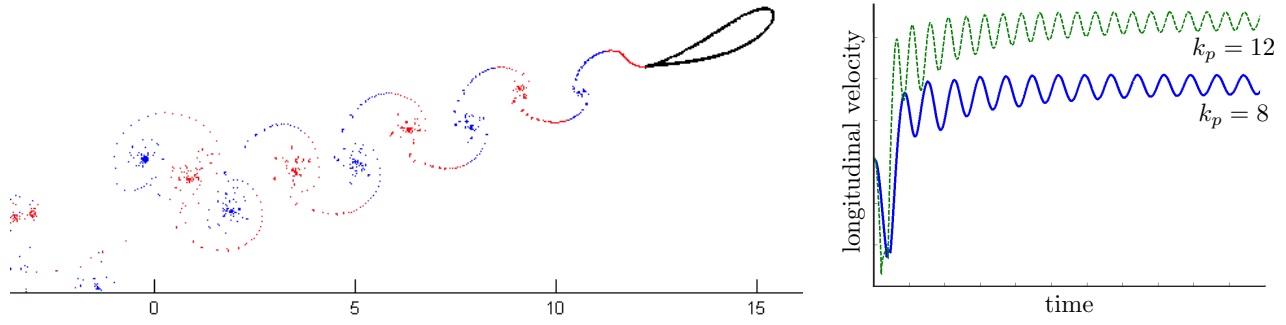


Figure 2. ACCELERATION FROM REST OF A FISHLIKE SWIMMER USING ITS CAMBER TO REGULATE ITS HEADING.

top was considered in [9], and our approach to the reduced-order modeling of the system — focusing on the evolution of the system’s *nonholonomic momentum* — is consistent with the discussion therein. Our version of the system differs from that in [9], however, in that the center of mass of our cart is not assumed to coincide with the point at which the wheel (or blade) contacts the ground. We limit ourselves, furthermore, to a single control input, and examine the dynamics of the system under continuously applied feedback control. In contrast, an algorithmic approach to steering is developed in [9] whereby the open-loop dynamics of the system are exploited through occasional control interventions involving two degrees of freedom in the position of the mass relative to the point of constraint. We examine motion generation in the sense of [7]; the theme of [9] is steering when propulsive momentum is already available.

Before proceeding, we note the qualitative similarity of our approach, in which a closed-loop system is constructed around a nonlinear plant so that the former behaves like a damped oscillator, to the formulation of PD control on Riemannian manifolds in [10] and related papers. A geometric analysis of our closed-loop system is forthcoming. We also note that our system complements the class of mobile wheeled inverted pendulums considered in [11] and related papers.

2.1 Modeling

Fig. 3 depicts the symbols we employ in modeling the system from Fig. 1. The wheel is assumed to align with the cart and to make contact with the ground along the cart’s rear edge. The point (x, y) represents the cart’s center of mass, about which the cart has rotational moment of inertia J . The longitudinal displacements a and b are constant, while the lateral displacement $c(t)$ of the mass relative to the cart is manipulated for control. The angle θ is measured between the laboratory-fixed x axis and the longitudinal axis of the cart.

We neglect the effect of friction on the cart-mass system, except in the sense that it proscribes lateral slipping of the wheel along the ground, and assume the system to obey Lagrange’s equations subject to the lateral force on the wheel that prosecutes the constraint. The Lagrangian is supplied by the total kinetic en-

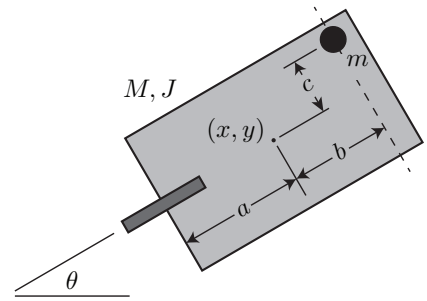


Figure 3. PARAMETERIZATION OF THE CART.

ergy

$$L = \frac{1}{2}M(\dot{x}^2 + \dot{y}^2) + \frac{1}{2}J\dot{\theta}^2 + \frac{1}{2}m(\dot{x}_m^2 + \dot{y}_m^2)$$

embodied in the motion of the cart and the motion of the mass, where

$$x_m = x + b \cos \theta - c \sin \theta, \quad y_m = y + c \cos \theta + b \sin \theta.$$

The motion of the system over time corresponds to a time-parametrized curve in the configuration manifold $Q = \mathbb{R} \times SE(2)$ such that vectors tangent to this curve annihilate the constraint form

$$\omega = -\sin \theta dx + \cos \theta dy - a d\theta. \quad (1)$$

The dynamics of the system are lower-dimensional than the configuration manifold. Given the system’s initial state, its subsequent behavior can be reconstructed completely from the time history of the displacement $c(t)$ together with the first-order dynamics of the system’s two-dimensional *nonholonomic momentum*, a concept developed in detail in [6]. A complete mathematical presentation of this concept is beyond the scope of the present paper, but the essential idea is straightforward to convey.

Consider the unconstrained motion of a rigid body in the plane — say, the cart in Fig. 3 with neither the wheel nor the additional mass present. The invariance of the cart’s kinetic energy under rigid translations and rotations of the laboratory frame of reference gives rise, via *Noether’s theorem* [12], to a three-dimensional conservation law. We may equate this with the independent conservation of linear momentum in the x direction, linear momentum in the y direction, and angular momentum about the origin of the xy plane, but this decomposition is partly arbitrary.

If the cart’s momentum is decomposed relative to a body-fixed frame — for instance, into longitudinal linear momentum, lateral linear momentum, and angular momentum about the cart’s center of mass — then the components of momentum will evolve over time as the body frame rotates relative to the laboratory frame. The equations governing the dynamics of these scalar momenta exemplify *Lie-Poisson equations*, analogous to Euler’s equations for the body-fixed angular momenta of a rigid body rotating about its center of mass in three dimensions [12]. The principle of *Hamiltonian reduction* is manifest in the fact that if the time histories of the momenta defined in the body frame are known, then the evolution of the body frame relative to the laboratory frame can be reconstructed after the fact — meaning that the dynamics of the momenta in the body frame encode the complete dynamics of the system.

The addition of the wheel to the cart in Fig. 3 breaks the symmetry in the system that engenders the conservation of three-dimensional momentum. Neither the linear momentum of the cart in the x direction, nor the linear momentum in the y direction, nor the angular momentum about the origin or about the cart’s center of mass is conserved with the wheel’s no-slip constraint in place. If the body frame is attached to the cart where the wheel contacts the ground, however, it’s apparent that the constraint opposes the evolution of only one of three components of momentum. The cart can have no lateral linear momentum, but can translate freely in the longitudinal direction, and can rotate freely about the center of the wheel.

The cart’s two-dimensional nonholonomic momentum represents the combination of linear and angular momenta that are permitted by the constraint to evolve freely at any instant in time. As the cart’s heading changes, the direction in which nonzero linear momentum is permissible — measured relative to the laboratory frame — also changes, but it’s always the case that two degrees of freedom exist in the cart’s momentum overall. As was the case in the absence of the constraint, we have freedom in choosing a decomposition of the evolving momentum into two scalar parts. This is equivalent to choosing a pair of vector fields on Q that span the space D_q of tangent vectors annihilating the one-form (1) at each $q \in Q$.

The simplicity of the nonholonomic momentum equations depends significantly on this choice of vector fields. For the

present system, physical considerations motivate us to define

$$D_q = \text{span} \left\{ -a \sin \theta \frac{\partial}{\partial x} + a \cos \theta \frac{\partial}{\partial y} + \frac{\partial}{\partial \theta}, \cos \theta \frac{\partial}{\partial x} + \sin \theta \frac{\partial}{\partial y} \right\},$$

consistent with [9]. Flow along the the first and second of these vector fields corresponds, respectively, to counterclockwise rotation of the cart about the wheel and to forward longitudinal translation. The two components of nonholonomic momentum defined below inherit their physical significance from these motion primitives. The exclusive reference of these interpretations to the body-fixed frame reflects the invariance of these vector fields under the left action of $SE(2)$ on Q corresponding to rigid translation and rotation of the laboratory frame. We now proceed according to the formalism developed in [6].

At each point $q \in Q$, the subspace of $T_q Q$ tangent to the orbit of the aforementioned $SE(2)$ action is given by

$$T_q(\text{Orb}(q)) = \text{span} \left\{ \frac{\partial}{\partial x}, \frac{\partial}{\partial y}, \frac{\partial}{\partial \theta} \right\}.$$

We define S_q to be the intersection of D_q with $T_q(\text{Orb}(q))$ at each point q , or

$$S_q = \text{span} \left\{ -a \sin \theta \frac{\partial}{\partial x} + a \cos \theta \frac{\partial}{\partial y} + \frac{\partial}{\partial \theta}, \cos \theta \frac{\partial}{\partial x} + \sin \theta \frac{\partial}{\partial y} \right\}.$$

We define

$$\mathfrak{g}^q = \{ \xi \in \mathfrak{se}(2) \mid \xi_Q(q) \in S_q \}$$

to comprise Lie algebra elements corresponding to infinitesimal generators of the $SE(2)$ action on Q that lie in S_q at the point q , and note that the vector fields we’ve chosen to appear in our definitions of D_q and S_q are such infinitesimal generators.

We denote the bundle over Q with fiber \mathfrak{g}^q at each point q by \mathfrak{g}^D and define the *nonholonomic momentum map* $J^{\text{nhc}} : TQ \rightarrow (\mathfrak{g}^D)^*$ such that

$$\langle J^{\text{nhc}}(v_q), \xi \rangle = \langle \mathbb{F}L(v_q), \xi_Q \rangle$$

for $\xi \in \mathfrak{g}^q$ and $v_q \in T_q Q$, where $\mathbb{F}L : TQ \rightarrow T^*Q$ denotes the Legendre transformation. Given a particular choice of ξ , we refer to either pairing above as the corresponding component p of the nonholonomic momentum, computed using local coordinates as

$$p = \frac{\partial L}{\partial \dot{q}^i}(\xi_Q)^i.$$

Corresponding to the Lie algebra elements that generate the two vector fields appearing in our definitions of D_q and S_q , we obtain the two components

$$\begin{aligned} p_1 &= (-mc \cos \theta - (bm + am + aM) \sin \theta) \dot{x} \\ &\quad + ((bm + am + aM) \cos \theta - mc \sin \theta) \dot{y} \\ &\quad + (J + m(ab + b^2 + c^2)) \dot{\theta} + m(a + b) \dot{c} \end{aligned}$$

and

$$p_2 = (m + M) \cos \theta \dot{x} + (m + M) \sin \theta \dot{y} - mc \dot{\theta}$$

of the nonholonomic momentum.

The evolution of the quantity p corresponding to a particular Lie algebra element $\xi \in \mathfrak{g}^{q(t)}$ is given, invoking local coordinates, by the *momentum equation*

$$\dot{p} = \frac{\partial L}{\partial q^i} \left[\dot{\xi} \right]_Q^i.$$

To illustrate the manner in which the time derivative of ξ may be nonzero as $q(t)$ evolves, we note that

$$\xi_Q = -a \sin \theta \frac{\partial}{\partial x} + a \cos \theta \frac{\partial}{\partial y} + \frac{\partial}{\partial \theta}$$

— the first vector field we've chosen to represent D_q and S_q — is the infinitesimal generator corresponding to the Lie algebra element

$$\xi = (y - a \sin \theta, -x + a \cos \theta, 1) \in \mathfrak{se}(2) \approx \mathbb{R}^3,$$

which changes from point to point in q . For the two components of nonholonomic momentum chosen above, it follows that

$$\dot{p}_1 = \frac{CD + EF}{G^2}, \quad \dot{p}_2 = \frac{HI}{G^2}, \quad (2)$$

where

$$\begin{aligned} A &= bm + am + aM \\ B &= J + (a + b)^2 + a^2M \\ C &= A(Bp_2 + mc(p_1 + p_2c - (a + b)m\dot{c})) \\ D &= -mp_2c + (m + M)(-p_1 + (a + b)m\dot{c}) \\ E &= m(B(m + M) + mM c^2) \\ F &= \dot{c}(-Bp_2 + mc(-p_1 - p_2c + (a + b)m\dot{c})) \\ G &= (B(m + M) + mM c^2)^2 \\ H &= (m + M)Ap_1 + mAp_2c + m((m + M)(J - abM) + mM c^2)\dot{c} \\ I &= -mp_2c + (m + M)(-p_1 + (a + b)m\dot{c}). \end{aligned}$$

2.2 Control

In the simulation depicted in Fig. 1, the lateral acceleration $\ddot{c}(t)$ of the mass relative to the cart is regarded as the control input, linked to the heading in the closed-loop system by the control law

$$\ddot{c}(t) = k_p (\theta(t) - \theta_{\text{desired}}(t)). \quad (3)$$

The top row in Fig. 4 revisits the simulation from Fig. 1 in more detail. Over time, the cart's heading exhibits decaying oscillations about the desired value while the translational speed of the cart's center of mass converges on a certain positive constant. The bottom row represents the behavior of the same cart with the same initial conditions but a different controller gain. Again, the cart converges upon the desired heading, but the final translational speed is roughly doubled. In both cases, oscillations in the lateral position of the mass decay as well, and the mass settles toward the neutral position.

Despite the promise of Figs. 1 and 4, it must be noted that the controller (3) provides performance like that shown under only a restricted set of circumstances. In particular, given the physical parameters listed in the caption of Fig. 4, sufficiently large step changes in the desired heading lead to instability in $c(t)$, and even for small changes in the desired heading the initial value of $c(t)$ must be chosen judiciously to achieve decaying oscillations about $c = 0$.

In the absence of analytical bounds on our controller's performance, we conclude this Section by observing that the closed-loop system's tendency to generate locomotion from rest in response to heading-angle error may be inferred directly from (2) and (3). Suppose that $p_1 = p_2 = \dot{c} = \dot{\theta} = 0$ initially. If the right-hand side of (3) is made nonzero, both \ddot{c} and \dot{c} will become nonzero, requiring the right-hand side of the second equation in (2) to become nonzero — meaning that the cart develops linear momentum as a result of the control action.

3 VARIABLE-CAMBER HYDROFOIL

3.1 Modeling

A thorough description of the model represented in Fig. 2 is beyond the scope of the present paper; a summary appears in [13] and the details appear in [14]. The model builds upon the Hamiltonian formulation developed in [15] for the equations governing the interaction of a free rigid body with a collection of point vortices in a planar ideal fluid, extended to accommodate a body with time-varying shape.

The shape of the foil is specified as the image of a circle under a time-varying Joukowski transformation, parameterized to provide area-preserving variations in camber. At regular small intervals in time, the Hamiltonian evolution of the system comprising the foil and the existing set of vortices is interrupted to enforce the requirement that smooth flow separation occur at the

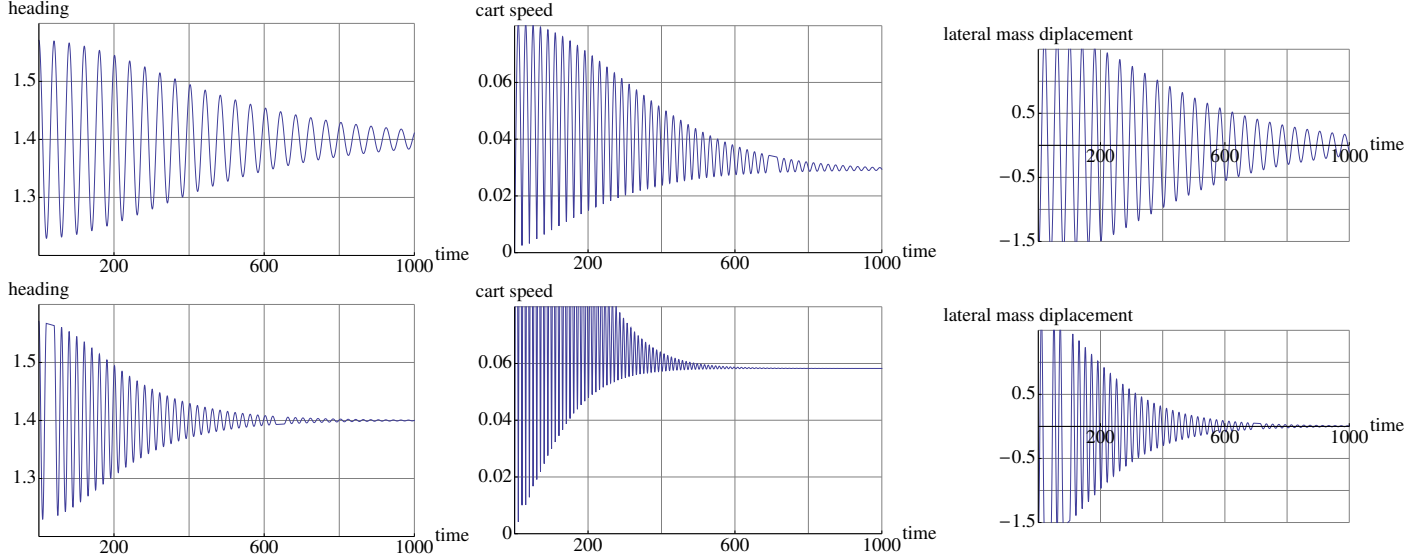


Figure 4. DYNAMICS OF THE CART WITH $a = 3$, $b = 2$, $M = 1$, $J = 4$, AND $m = 1/2$ SUBJECT TO THE CONTROL LAW (3) WITH $k_p = .25$ (TOP ROW) AND $k_p = 1$ (BOTTOM ROW). DIFFERENCES IN THE FEEDBACK GAIN LEAD TO DIFFERENCES IN THE FINAL ROLLING SPEED.

foil’s trailing point. This is achieved through the introduction of a new vortex near the foil’s trailing point to correct the flow, the concurrent amendment of the circulation around the foil to preserve Kelvin’s circulation theorem, and the concurrent amendment of the foil’s linear and angular velocity to preserve the total Kelvin impulse. The conservation of circulation and the conservation of impulse in ideal fluid–body systems are related to underlying symmetries. The latter corresponds to an $SE(2)$ symmetry like that of the Lagrangian and constraint distribution for the cart-mass system, leading to the conservation of linear and angular momentum by the cart in the absence of the wheel. The former corresponds to the particle-relabeling symmetry of the fluid kinetic energy, as discussed in [16].

Individual vortices in our model vary in orientation according to the flow conditions under which they’re shed from the foil’s trailing tip. Once shed, each vortex remains constant in strength and orientation. In real fishlike swimming, vortex shedding occurs as a result of fluid viscosity, which also contributes to the subsequent decay of shed vortices. Our goal in developing the present model was to preserve as much as possible of the geometric structure present in truly inviscid swimming — see [17, 18] — while capturing the single viscous phenomenon most relevant to locomotion.

3.2 Control

As noted in Section 1, simulations consistently indicate that the coupling of heading error to the rate of change of the foil’s camber through a single proportional gain is sufficient to enable the foil to track large step changes in the desired heading with zero average steady-state error. Given the dimensionality and nonlinearity of the dynamics through which the foil’s cam-

ber influences its heading, this is a surprising testament to the ambit of simple linear control. The authors documented the efficacy of PID heading control for this system in [19], which includes frames from an animation of the foil successfully tracking a 180-degree step change in desired heading alongside data representing less aggressive maneuvers. The focus of [19] is not the propulsive rectification of oscillations in heading, however, but rather the use of heading control as a means to harvest propulsive energy from ambient vorticity. The omission of derivative and integral terms from the feedback loop alters the oscillatory dynamics of the foil’s camber as the foil tracks a piecewise-constant desired heading.

Fig. 2 illustrates the acceleration of the foil through a sudden turn; Fig. 5 depicts the deceleration of the foil in response to a step change in the gain k_p when the desired heading remains unchanged. The two frames on the left portray the adjustment in the foil’s gait that takes place when k_p is decreased abruptly from 12 to 1. The initial conditions in Fig. 5 are precisely those from Fig. 2; the foil is initially at rest, aligned with the horizontal axis. The upper left panel shows the foil just before the change in k_p , after the foil has begun swimming in response to a change in the desired heading. The vortex pair above and to the left of the foil was shed in the initial moments of the simulation, when the foil gave its first propulsive kick.

The lower left panel shows the foil after the change in k_p . In order to slow its translation, the foil has executed a transition between a *pumping gait* and a *cruising gait*. The difference between the two is evident in the structure of the foil’s wake. The upper right panel depicts the longitudinal velocity of the foil as a function of time throughout the simulation generating the panels on the left.

The translational velocity of the foil settles about a new con-

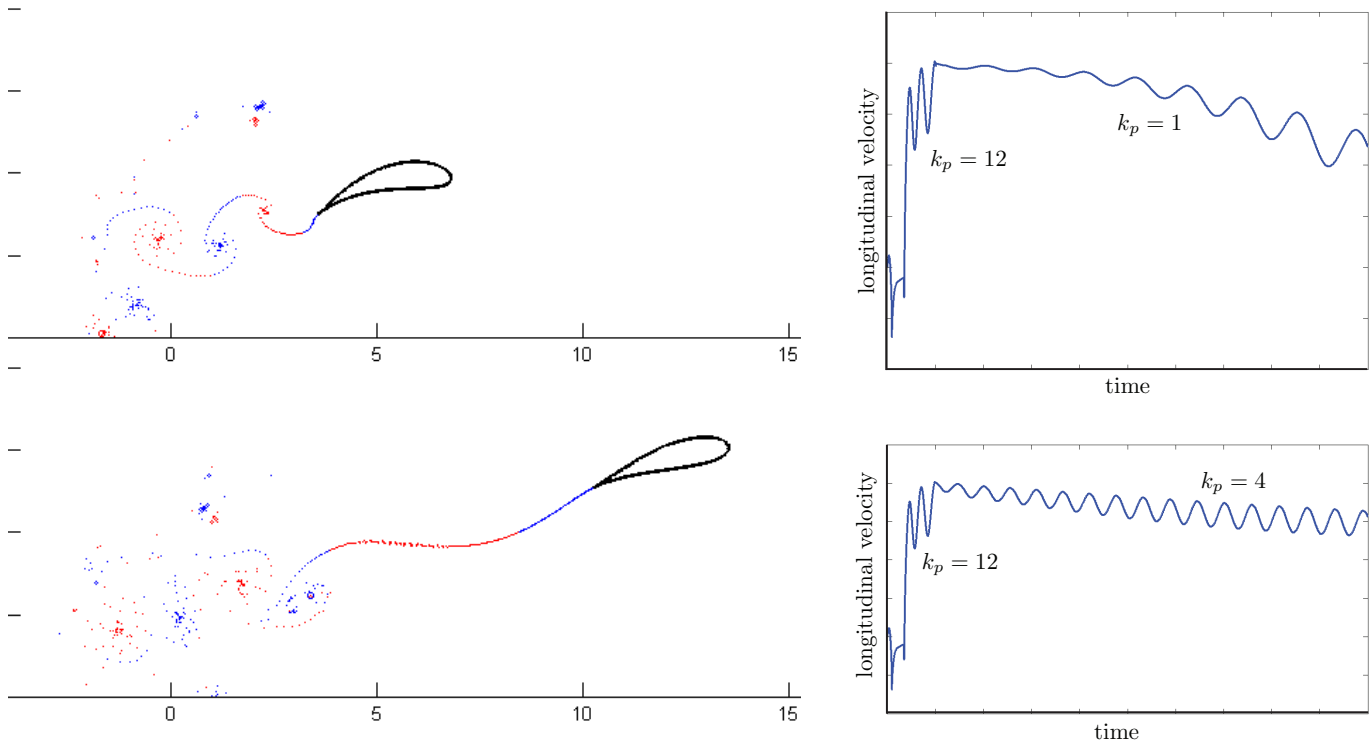


Figure 5. DECELERATION OF THE FOIL, WITHOUT TURNING, IN RESPONSE TO A DECREASE IN THE FEEDBACK GAIN.

stant value only after many oscillations. The panel on the lower right of Fig. 5 depicts the more rapid settling that occurs in response to a less significant change in k_p , from 12 to 4.

4 FUTURE WORK

The authors' immediate priority is to evaluate the applicability of the controllers described in Sections 2 and 3 to the control of physical vehicles. The left panel in Fig. 6 depicts a pair of robotic vehicles to be used for this purpose. The solitary rear wheel of the idealized cart has been replaced by a pair of wheels with a wide axle to ensure roll stability, but the dynamic constraint imposed by the pair of wheels is equivalent to that of the single wheel. The robotic hydrofoil comprises three rigid segments with individually actuated joints between them, fitted together to provide a smooth outer surface with variable camber. The foil floats upright in water, its upper face flush with the water's surface, and is modeled by the Joukowski foil from Fig. 2 when viewed from above.

The right panel in Fig. 6 depicts a NaturalPoint OptiTrack motion-capture system to be used for data collection with both robots. Eleven cameras are shown along the edges of the pool in which the hydrofoil will be deployed. The vertical antenna visible atop the foil enables wireless communication between the foil and the LabView-equipped PC connected to the OptiTrack system.

5 ACKNOWLEDGMENTS

The authors thank Tapobata Bhattacharya and Scott DeVoto for their comments and encouragement. Support for this work was provided in part by NSF grants CMMI 0822817, CMMI 1000652, and CMMI 1000656.

REFERENCES

- [1] Kelly, S. D., and Hukkeri, R. B., 2006. "Mechanics, Dynamics, and Control of a Single-Input Aquatic Vehicle With Variable Coefficient of Lift". *IEEE Transactions on Robotics*, **22**(6), pp. 1254–1264.
- [2] Childress, S., 1981. *Mechanics of Swimming and Flying*. Cambridge University Press.
- [3] von Kármán, T., and Burgers, J. M., 1934. *General Aerodynamic Theory: Perfect Fluids*, Vol. II of *Aerodynamic Theory*. Springer-Verlag.
- [4] Murray, R. M., and Sastry, S., 1993. "Nonholonomic Motion Planning: Steering Using Sinusoids". *IEEE Transactions on Automatic Control*, **38**(5), pp. 700–716.
- [5] Kelly, S. D., and Murray, R. M., 1995. "Geometric Phases and Robotic Locomotion". *Journal of Robotic Systems*, **12**, pp. 417–431.
- [6] Bloch, A. M., Krishnaprasad, P. S., Marsden, J. E., and Murray, R. M., 1996. "Nonholonomic Mechanical Systems with Symmetry". *Archive for Rational Mechanics and*

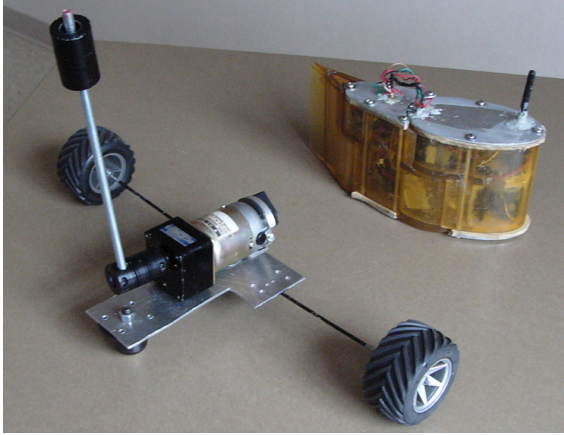


Figure 6. A ROBOTIC CART AND VARIABLE-CAMBER HYDROFOIL (LEFT) AND AN ARRAY OF CAMERAS ALONG TWO EDGES OF A POOL FOR OPTICAL MOTION TRACKING (RIGHT).

Analysis, **136**, pp. 21–99.

- [7] Ostrowski, J. P., 2000. “Steering for a Class of Dynamic Nonholonomic Systems”. *IEEE Transactions on Automatic Control*, **45**(8), pp. 1492–1498.
- [8] Chaplygin, S. A., 1911. “On the Theory of Motion of Non-holonomic Systems. The Theorem on the Reducing Multiplier”. *Matematicheskii Sbornik*, **28**(1).
- [9] Osborne, J., and Zenkov, D. V., 2005. “Steering the Chaplygin Sleigh by a Moving Mass”. In Proceedings of the 44th IEEE Conference on Decision and Control and European Control Conference, pp. 1114–1118.
- [10] Bullo, F., and Murray, R. M., 1999. “Tracking for Fully Actuated Mechanical Systems: A Geometric Framework”. *Automatica*, **35**(1), pp. 17–34.
- [11] Li, Z., and Luo, J., 2009. “Adaptive Robust Dynamic Balance and Motion Controls of Mobile Wheeled Inverted Pendulums”. *IEEE Transactions on Control Systems Technology*, **17**(1), pp. 233–241.
- [12] Marsden, J. E., and Ratiu, T. S., 1999. *Introduction to Mechanics and Symmetry*, 2nd ed. Springer-Verlag.
- [13] Kelly, S. D., and Xiong, H., 2010. “Self-Propulsion of a Free Hydrofoil with Localized Discrete Vortex Shedding: Analytical Modeling and Simulation”. *Theoretical and Computational Fluid Dynamics*, **24**(1), pp. 45–50.
- [14] Xiong, H., 2007. “Geometric Mechanics, Ideal Hydrodynamics, and the Locomotion of Planar Shape-Changing Aquatic Vehicles”. PhD thesis, University of Illinois at Urbana-Champaign.
- [15] Shashikanth, B. N., 2005. “Poisson Brackets for the Dynamically Interacting System of A 2D Rigid Cylinder and N Point Vortices: the Case of Arbitrary Smooth Cylinder Shapes”. *Regular and Chaotic Dynamics*, **10**(1), pp. 1–14.
- [16] Marsden, J. E., and Weinstein, A., 1983. “Coadjoint Orbits, Vortices, and Clebsch Variables for Incompressible Fluids”. *Physica 7D*, pp. 305–323.
- [17] Kelly, S. D., and Murray, R. M., 1996. “The Geometry and Control of Dissipative Systems”. In Proceedings of the 35th IEEE Conference on Decision and Control.
- [18] Kanso, E., Marsden, J. E., Rowley, C. W., and Melli-Huber, J. B., 2005. “Locomotion of Articulated Bodies in a Perfect Fluid”. *Journal of Nonlinear Science*, **15**, pp. 255–289.
- [19] Kelly, S. D., and Pujari, P., 2010. “Propulsive Energy Harvesting by a Fishlike Vehicle in a Vortex Flow: Computational Modeling and Control”. In Proceedings of the 49th IEEE Conference on Decision and Control.